Research Article

Chemically Activated Spruce Organosolv Lignin as a Carbocatalyst for Heterogeneous Oxidative Dehydrogenations in the Liquid Phase

Anna Lenarda, Michele Melchionna, Santeri Aikonen, Tiziano Montini, Paolo Fornasiero, Tao Hu, Michael Hummel, and Juho Helaja*

Read Online

| ACCESS | | Metrics & More | | Article Recommendations | | Supporting Information |

ABSTRACT: Activated carbons obtained from organosolv lignin by chemical activation with KOH and oxidized with diluted HNO_3 were studied as catalysts for aerobic oxidative dehydrogenation (ODH) reactions. The structure/ activity relationship was investigated through multiple techniques revealing the crucial role of oxygen functionality distribution in promoting two mechanistically archetypical ODH probe reactions: (i) the tetrahydroquinoline (THQ) aromatization, which represents ODH triggered by hydride transfer, and (ii) the 2-phenyl indole homocoupling reaction, a model for single-electron transfer-promoted reactions. In particular, the catalytic activity, correlating with oxygen functionality distribution on the basis of X-ray photoelectron spectroscopy and temperature-programmed desorption analysis, was associated with the C=O surface functionalities, as confirmed by blocking experiments with 2,2,2-trifluoroethyl hydrazine. Kinetic profiling tools were employed to assess THQ ODH product inhibition effects on the overall yield of the process as well as the extent of stoichiometric activity of the carbocatalyst. The breadth of the developed catalysts' applicability was explored through selected relevant ODH reactions.

KEYWORDS: heterogeneous catalysis, carbon materials, lignin, organocatalysis, oxidative dehydrogenation
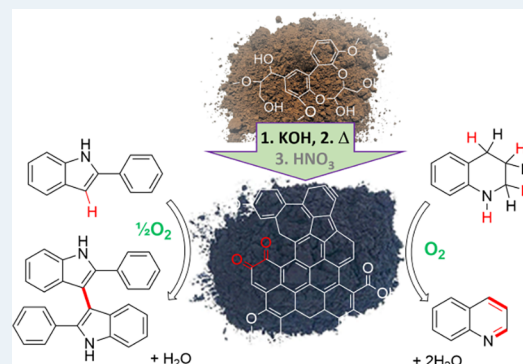
■ INTRODUCTION

Carbon-based materials have shown great potential as an alternative to metals to promote various organic transformations, in particular oxidative dehydrogenation (ODH) reactions of organic compounds.[1−3] Because of their metal-free nature, heterogeneous carbocatalysts are an attractive alternative in ODH catalysis, not only because they can replace air- and sulfur-sensitive metal catalysts, which suffer from facile deactivation, but also because they can be used as substitutes for rare metal-based catalysts, which are limited by global resources. In the past three decades, several metal-free systems based on the so-called carbon nanostructures (CNS) have been developed. Nanosized materials, such as carbon nanotubes (CNTs), graphene, carbon nanohorns (CNHs), nanodiamonds, fullerenes, asphaltene oxides, or carbon nanodots, are currently at the cutting edge of carbocatalyst design.[4] The catalytic activity of such materials is usually associated with the presence of defective sites in the graphitic 2D domains, the presence of oxygen functionalities, and, in some cases, other heteroatom dopants.[5,6]

In particular, in many studies on ODH catalysis, quinoidic/ carbonyl groups have been identified as the most probable active sites (Figure 1).[6,7] Nanocarbons' improved tensility, crystallinity, geometric definition, and durability have made their application to ODH reactions successful, achieving high

catalytic efficiency,[8] at the expense, unfortunately, of their high cost and complex production protocols. Graphene oxide (GO) has been recently a popular carbonaceous catalyst and reagent to mediate various, mostly acid catalyzed, organic transformations in the liquid phase.[9] Still, very little information exists on the interaction of nanocarbon materials with living organisms, making it hard to determine their toxicity both for humans and for the environment.[10]

By contrast, activated carbons (ACs) are known for their wide availability and cheapness as well as their lower levels of health and environmental hazards. ACs' role in catalysis stems from their properties, which include a large surface area, well developed porosity, and surface chemistry rich in oxygen groups and defective sites.[11] Their catalytic activity has been known since 1855 when ACs were reported to catalyze the oxidation of a mixture of organic gases coming from putrefied biomass. Later on, ACs have been employed to catalyze the gas phase ODH of ethylbenzene and light alkanes, and the
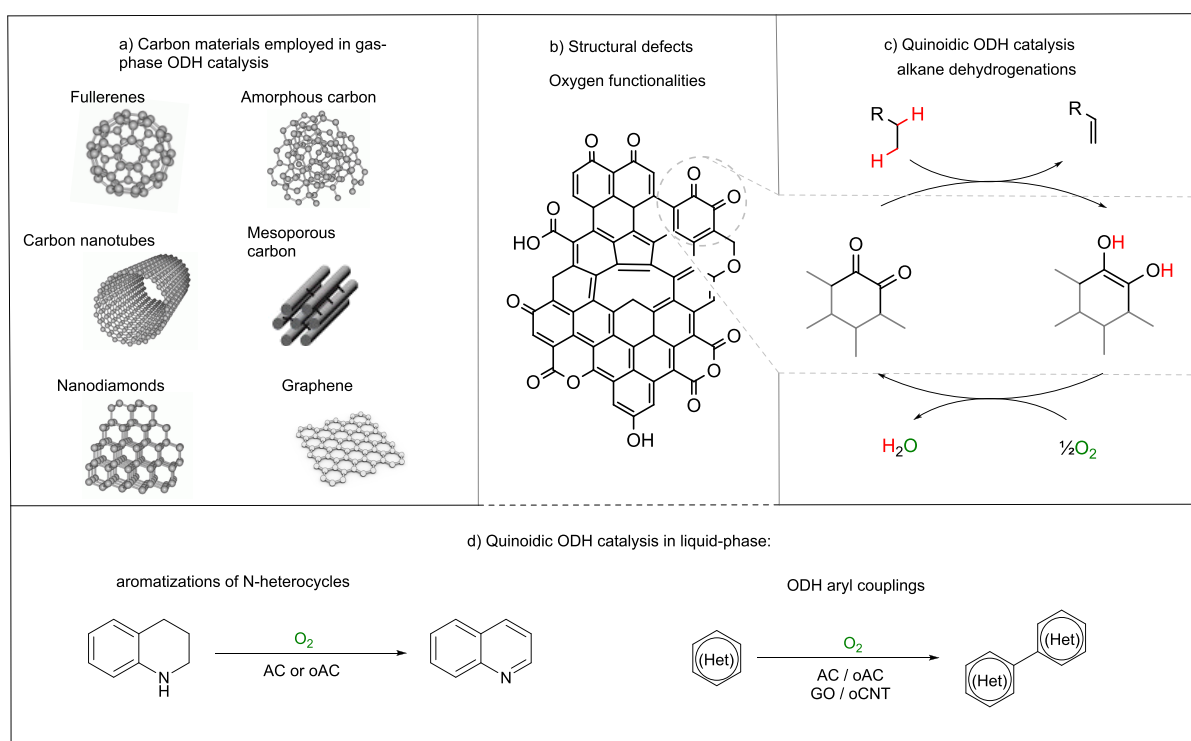
Figure 1. Various carbon materials have shown catalytic activity in ODH reactions: (a) carbon materials applied in gas phase dehydrogenation of alkenes, (b) possible defects and O-functional groups, (c) quinoidic redox cycle, and (d) liquid phase ODH reactions.[1]
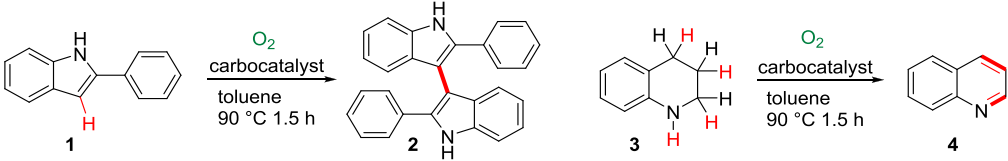
quinoidic oxygen centers have been proposed to be the active sites in these types of chemical conversions.[12] In the liquid phase, Hayashi has employed ACs under mild oxidative conditions to achieve various ODH reactions, in particular aromatizations of N-heterocycles.[13] Our previous work in this field demonstrated that by increasing the oxygen content of commercially available AC via HNO_3 or thermal air oxidation, the resulting oxidized ACs (oACs) exhibit higher catalytic activity in both ODH aromatization and coupling reactions (Figure 1c).[14−17]

As a catalytic material, ACs include however some noticeable shortcomings, likely due to their lack of three-dimensional order and amorphous or disordered character. These features arise from the random bonding of small, defective graphene layers (sp^2 carbon) with linear carbon atoms (sp^3), which creates an imperfect packing, yet giving rise to a highly porous structure.[18] Also, ACs are industrially manufactured mainly for adsorption purposes, either of gases or pollutants in water purification.[19] Their performance is therefore normally enhanced in the presence of a large quantity of micropores. While beneficial for adsorption, the small cavities jointly with the long-range disordered structure can be detrimental for liquid phase catalysis, often leading to catalyst susceptibility to deactivation.[20] Moreover, active carbons prepared from natural precursors are prone to contain metallic impurities (Mo, Co, Fe, Ni, and Cu), which are intrinsic to the starting material and are rather difficult to remove completely.[21] This feature poses the notorious challenge of unequivocal identification of the catalytically active sites. In our vision, the availability of a synthetic method able to produce ACs specifically tailored for specific tasks, with a high catalytic activity, totally free from metal impurities and with high levels of batch reproducibility would be of very wide interest in carbon material development.

Many bottom-up carbonization methods have been developed for porous catalytically active carbon materials.[22] This approach is promising as the introduced heteroatoms can function as active sites for various catalytic applications. Bottom-up carbonization methods, however, can present scalability and sustainability problems depending on the carbon source and necessity of metal catalysis.[22] Carbonization of biomass-derived polymers has attracted attention as an efficient strategy to produce catalytic carbon materials in a more economic and ecologic way.[23] Kraft lignin was recently reported as a promising carbon source to produce catalytically active graphene-like materials to be employed in oxidation reactions.[24] In this case, however, the impurity characteristic of this type of lignin, consisting mostly in S-containing and metal ions, is implied to be the driving force both for the development of structural features of the produced carbon materials and for the catalytic activity displayed. For the present study, we chose spruce lignin obtained by an organosolv process, a more environmentally friendly pulping technique that employs an organic solvent to solubilize lignin, as it is free of impurities and can serve as a model to build a general, strategic protocol for biomass utilization.
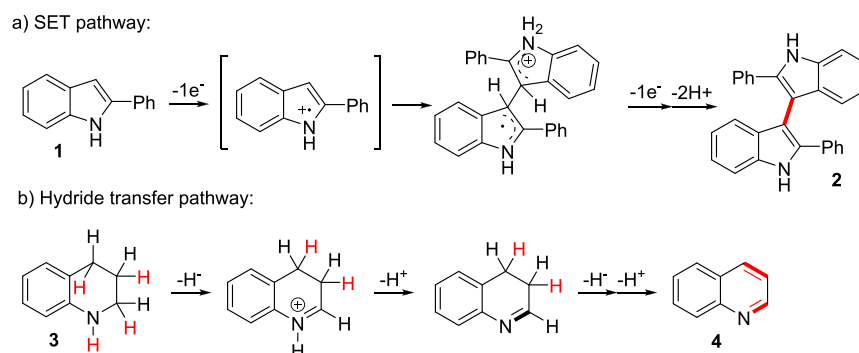
Chemical activation was chosen as the pore generation method as it proceeds in a single step and at lower temperatures, making it less energy- and time-consuming than physical activation.[25,26] More so, the process of chemical activation of biomass with alkali hydroxides has been studied thoroughly and is reported to provide materials with high values of surface areas and pore volumes, combined with the development of oxygenated functionalities.[27]

In the work at hand, we have developed carbocatalysts from organosolv spruce lignin with enhanced and task-specific activity toward two different ODH reactions, which we have discovered in our previous works as models for different

Table 1. Catalytic Activity Tests of Carbon Materials for ODH Coupling and Aromatization Reactions[g]

entry	catalysts	1 to 2 yield [%][a,e]	3 to 4 yield [%][a,e]	entry	catalysts	1 to 2 yield [%][a,e]	3 to 4 yield [%][a,e]
1	oLAC-1-700	20 (40)	52 (72)	11	rGO[c]	12 (19)	22 (42)
2	oLAC-2-700	35 (48)	60 (75)	12	AC[d]	6 (10)	7 (20)
3	oLAC-3-700	50 (65)	52 (70)	13	oAC$_{HNO3}$[d]	35 (50)	21 (39)
4	oLAC-1-800	44 (63)	44 (61)	14	oAC$_{air}$[d]	33 (46)	37 (50)
5	oLAC-2-800	43 (60)	50 (68)	15	oAC$_{air(\Delta)}$[d]	23 (30)	36 (47)
6	oLAC-3-800	60 (70)	39 (55)	16	oAC$_{HNO3dil}$[d]	30 (41)	13 (30)
7	oLAC-1-900	57 (67)	42 (58)	18	LAC-0-700	0 (-)	0 (-)
8	oLAC-2-900	51 (64)	47 (63)	19	oLAC-0-700	0 (-)	0 (-)
9	oLAC-3-900	65 (72)	39 (52)	20	oLAC-3-900[f] F-blocked	9 (17)	
10	GO[b]	22 (50)	13 (28)	21	oLAC-2-700[f] F-blocked		14 (31)

[a]Measured with ^{1}H NMR using 1,3,5-trimethoxybenzene standard, average of two runs. [b]Graphene oxide, few layer modified Hummer's (Cheaptubes.com). [c]Reduced graphene oxide (rGO), S.A: 1562 m^2 g^{-1}, two to five layers (nanografi.com). [d]1 kg batch (Lot. H2430) from Fluka with 100 mesh particle size. [e]Values in parenthesis report % conversion values. [f]2,2,2-Trifluoroethyl hydrazine labeled.[31] [g]Catalyst loading (defined as 1 equiv) 224 mg/mmol, 0.1 mmol substrate, and 1 mL of toluene as in ref 14.

Scheme 1. Mechanistic Pathways Proposed for the Studied ODH Reactions[a]

[a](a) Coupling of 2-phenyl indole via the SET pathway and (b) aromatization of THQ via hydride transfer.

carbocatalytic oxidative mechanistic paths: single-electron transfer (SET) and hydride abstraction.[14−17] We observed that the specific activity can be tuned by varying crucial parameters in the preparation protocol, which influence directly the morphologic and functional properties of the materials in terms of pore size and oxygen-containing group distribution. In the case of amorphous carbon materials, it is challenging to evaluate the effect of the structural properties on the catalytic activity: we have analyzed their dependence by combining material characterization techniques with experimental kinetics and mechanistic studies and verified them by exploring the materials' activity in a wide variety of known ODH reactions.

RESULTS AND DISCUSSION

We selected KOH as the activating agent because its mechanism of action has been studied thoroughly: by reviewing the literature on the topic, the temperature and the ratio between the chemical agent and lignin were selected as the most influential parameters for tuning the development of porosity in the generated active carbons.[28] The temperature treatment was conducted between 700 and 900 °C: as reported in a recent study,[29] in fact, at temperatures higher than 700 °C,

the micropores initially formed at lower temperatures (350−400 °C) start to widen, leading to the formation of larger ones, with the anticipated advantage of facilitating reagent diffusion during liquid phase catalysis. One-stage pyrolysis, without pre-carbonization, was preferred as it reduces the preparation steps and the overall environmental impact and economic cost and has been reported to produce a better porous structure.[30] We varied the conditions as follows (Table S2): lignin was impregnated with KOH at 1:1, 2:1, and 3:1 ratios and pyrolyzed in a horizontal tubular oven for 3 h at 700, 800, or 900 °C under an Ar atmosphere, respectively, and subsequently washed with HCl and water. The samples were named LAC-X-YYY where X is the weight equivalent of KOH and YYY is the pyrolysis temperature. A portion of each lignin active carbon sample was then oxidized with diluted nitric acid employing a procedure suitable to obtain the optimal degree of functionalization with oxygen-containing groups and the lowest structural damage on the surface.[31] Each oxidized sample oLAC-X-YYY was tested as the catalyst in two known model reactions involving different types of dehydrogenation events (Table 1): (a) the oxidative homocoupling of 2-phenyl indole to 3,3′-biindole[14] and (b) the (aromatizing) dehydrogenation of tetrahydroquinoline to quinoline.[15] Our previous

studies suggest that both ODH reactions are promoted by the quinone surface groups present on the carbon, but while homocoupling is mediated by one-electron (SET) oxidation of the substrate by the quinoidic moieties, in THQ aromatization, the quinone act as a hydride acceptor (Scheme 1). These different mechanistic pathways suggest that specific structural features could promote each transformation preferentially, so they could be tailored to reach optimal catalytic performance. Commercial GO and rGO were employed as reference catalysts.[2,3,9] Moreover, some commercial active carbons oxidized in different ways were screened as terms of comparison, including AC oxidized with the same protocol used for the other lignin-derived materials ($oAC_{HNO3dil}$), AC oxidized under air ($oAC_{air(\Delta)}$),[15] and AC oxidized with concentrated nitric acid (oAC_{HNO3}),[14] the latter two materials already reported by our group as ODH catalysts. To have a meaningful comparison of the catalysts' intrinsic activity, the reaction was stopped after 90 min so that for each catalytic test, the reaction was still far from reaching complete conversion (conversion after 90 min ranges between 20 and 75% depending on the catalyst and conditions). The reactions proceeded cleanly as no side products were detected by ^{1}H-NMR, and the mismatch between product yield and substrate conversion is likely due to the chemical or physical absorption of the reagents on the carbon surface. The results obtained are summarized in Table 1.

Remarkably, the newly designed lignin-derived carbocatalysts exhibited moderate to high activity for both the investigated reactions outperforming GO and rGO as well as our previously reported top performing oxidized commercial activated carbons oAC_{HNO3} for the indole homocoupling[14] and $oAC_{air(\Delta)}$ for the aromatization of THQ.[15]

Importantly, the screening evidenced dramatically different activity trends for the two reactions: the oxidative homocoupling of 2-phenyl indole appears to be promoted by carbons treated at high temperature and with high amounts of base, whereas the dehydrogenation of tetrahydroquinoline seems to benefit from carbocatalysts prepared under milder conditions, opening the possibility to tailor the properties of lignin-derived active carbons to make them task-specific.

To establish the relevance of every step of the treatment and understand the reason for this behavior, additional tests were performed with a series of carbons before nitric acid treatment, and as a reference, with lignin carbonized at 700 °C in the absence of KOH (LAC-0-700) and subsequently treated with nitric acid (oLAC-0-700). The results obtained are reported in Table 1. As expected, no catalytic yield was observed using either LAC-0-700 or oLAC-0-700, confirming that KOH is indeed crucial in producing catalytically active materials. Moreover, HNO_3 treatment was ineffective in improving the catalytic performance of this material. This is not surprising as lignin carbonization in the absence of an activating agent does not allow the development of the suitable porosity needed for the catalytic events to take place.[32,33] The best performing carbon materials for each reaction, oLAC-2-700 and oLAC-3-900, were also tested prior to the HNO_3 treatment. While LAC-3-900 shows very low activity toward the homocoupling reaction (4%), LAC-2-700 has proven to be able to catalyze with significant activity (60%) the THQ aromatization reaction. We can assume that the acid treatment has a bigger influence in the former case because of the known ability of acidic groups in promoting the aryl coupling reaction.[14,34] The full dataset for the catalytic activity of the carbon materials

before HNO_3 oxidation, exhibiting a similar trend, is reported in Table S3. Some materials were also prepared employing NaOH instead of KOH as the activating agent (Table S4). As none of them reached the activity of the top performing materials prepared with KOH, the latter base was preferred for the study.

Structure/activity relationship was first investigated by analyzing the surface oxygen group type and distribution and textural properties of the materials. The textural properties of the whole dataset were studied through N_2 physisorption using the Brunauer−Emmett−Teller (BET) model for surface area determination (Figures S1−S3). The relevant parameters are reported in Table 2. XPS spectra were recorded for the whole

Table 2. BET Analysis Parameters and XPS O% Content for the Full Dataset

sample	BET surface area m^2 g^{-1}	external surface area m^2 g^{-1}	microporous surface area m^2 g^{-1}	microporous volume m^2 g^{-1}	O% content
oLAC-1-700	957	75	882	0.339	17.3
oLAC-2-700	1038	86	956	0.374	15.6
oLAC-3-700	1698	661	1037	0.341	13.2
oLAC-1-800	1283	283	1000	0.355	12.8
oLAC-2-800	1222	302	920	0.323	12.0
oLAC-3-800	1961	1324	637	0.117	10.3
oLAC-1-900	1477	503	974	0.326	10.9
oLAC-2-900	1514	559	982	0.301	11.8
oLAC-3-900	2104	1230	874	0.171	10.7

dataset before and after HNO_3 treatment and deconvoluted using literature parameters (Figures S4−S9).[6] For the C1s peak, six components were identified, sp^2-C (284.6 eV), sp^3-C (285.2 eV), C−O (286.1 eV), —C=O (287.6 eV), —O—C=O (289.1 eV), and $\pi-\pi^*$ stacking (291.3 eV) while the O1s peak has been deconvoluted isolating three contributions, C−O (533.2 eV), C=O (531.51 eV), and an additional broad band at 535.8 eV accounting for chemisorbed oxygen.[6] Figure 2 shows the correlation of the catalytic performance of each material and the relevant morphologic or functional surface feature.

As a general trend, we can observe that samples treated at higher temperature and with higher amounts of KOH display a higher BET surface area, consisting mainly in meso- and macropores, and lower overall oxygen content as shown in our X-ray photoelectron spectroscopy (XPS) data (Table S5).

This effect is in line with most studies on the mechanism of carbon materials activation by KOH.

Notably, a recent study focusing on the reactions occurring during one-stage biomass activation by KOH suggests that the process starts with the activating agent first reacting with O-containing groups in the original structure followed by reaction at higher temperature (higher than 600 °C) with the carbon fragments creating vacancies, where OH$^-$ enters and forms
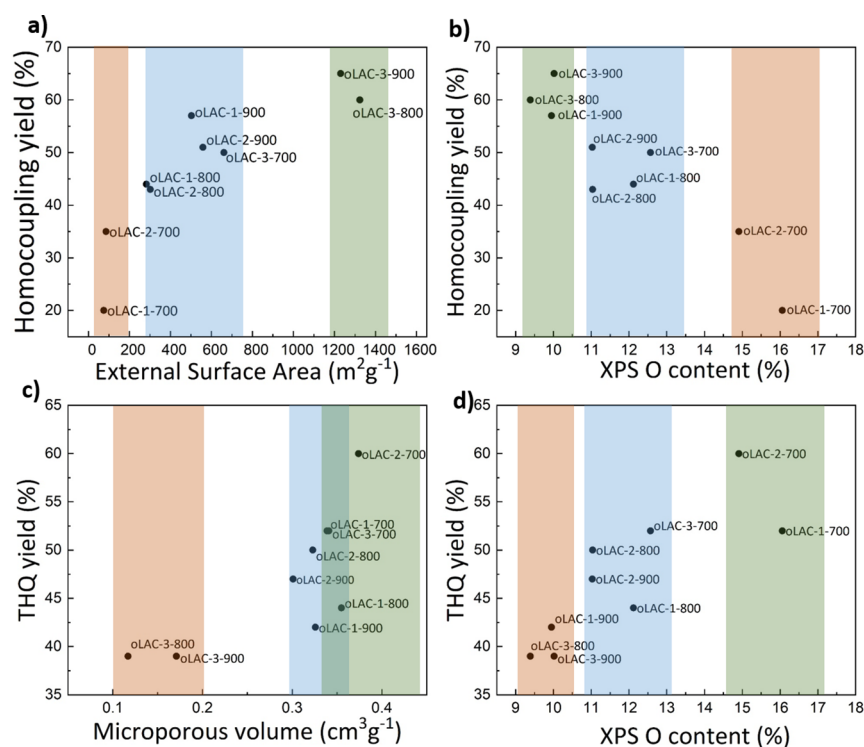
Figure 2. Percent yield of (a) homocoupling versus external surface area and (b) versus O% content (XPS); percent yield of (c) THQ aromatization versus microporous volume and (d) versus O% content (XPS), under aerobic conditions, after a 1.5 h reaction time. Colored bars evidence the best (green), average (blue), and worst (orange) performing samples.
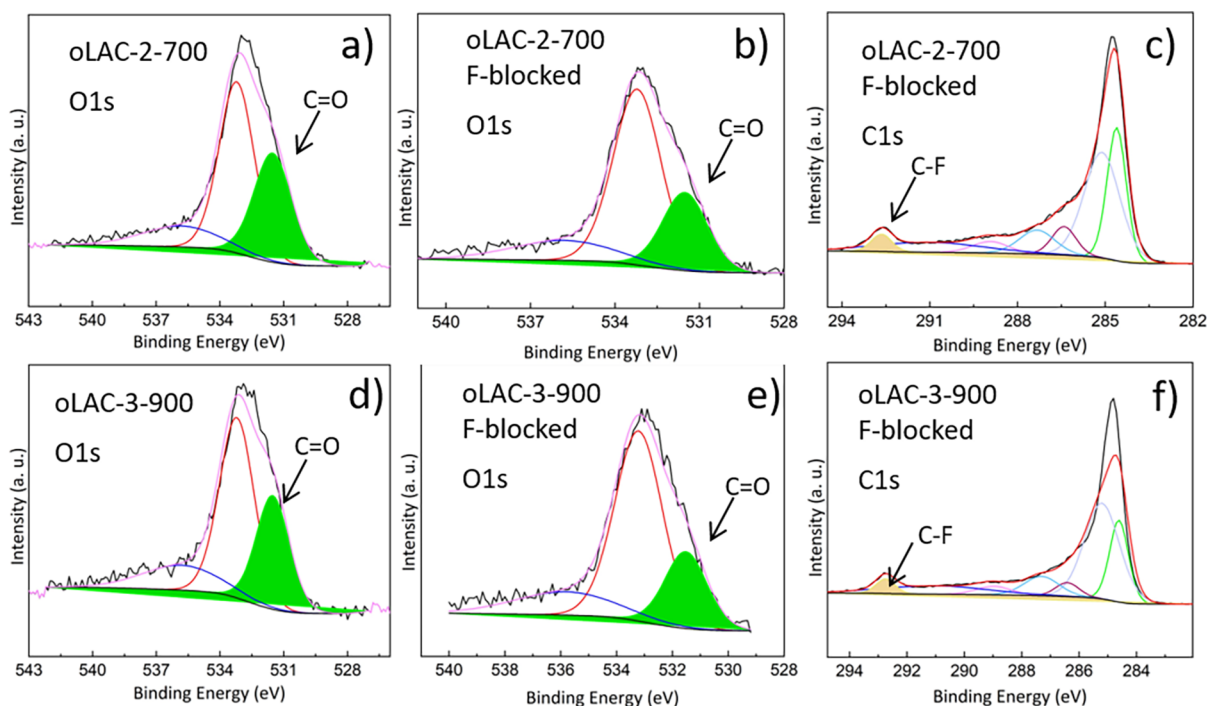

Figure 3. O1s spectra of (a) oLAC-2-700, (b) oLAC-2-700 F-blocked, (d) oLAC-3-900, and (e) oLAC-3-900 F-blocked and C1s spectra of (c) oLAC-2-700 F-blocked and (f) oLAC-3-900 F-blocked.

new oxygen-containing groups. The high amount of oxygen in the materials obtained at 700 °C is presumably related to this stage of the process. At higher T and KOH loading, these groups start to be eroded, increasing the surface area and lowering the O content.[29]

The textural properties of the materials, obtained with different activation parameters, suggest a correlation with the different activity toward the explored reactions. The increase in external surface area occurring when 3 equiv of base is employed at every given temperature, leading to the formation of larger pores, can be associated with the higher catalytic
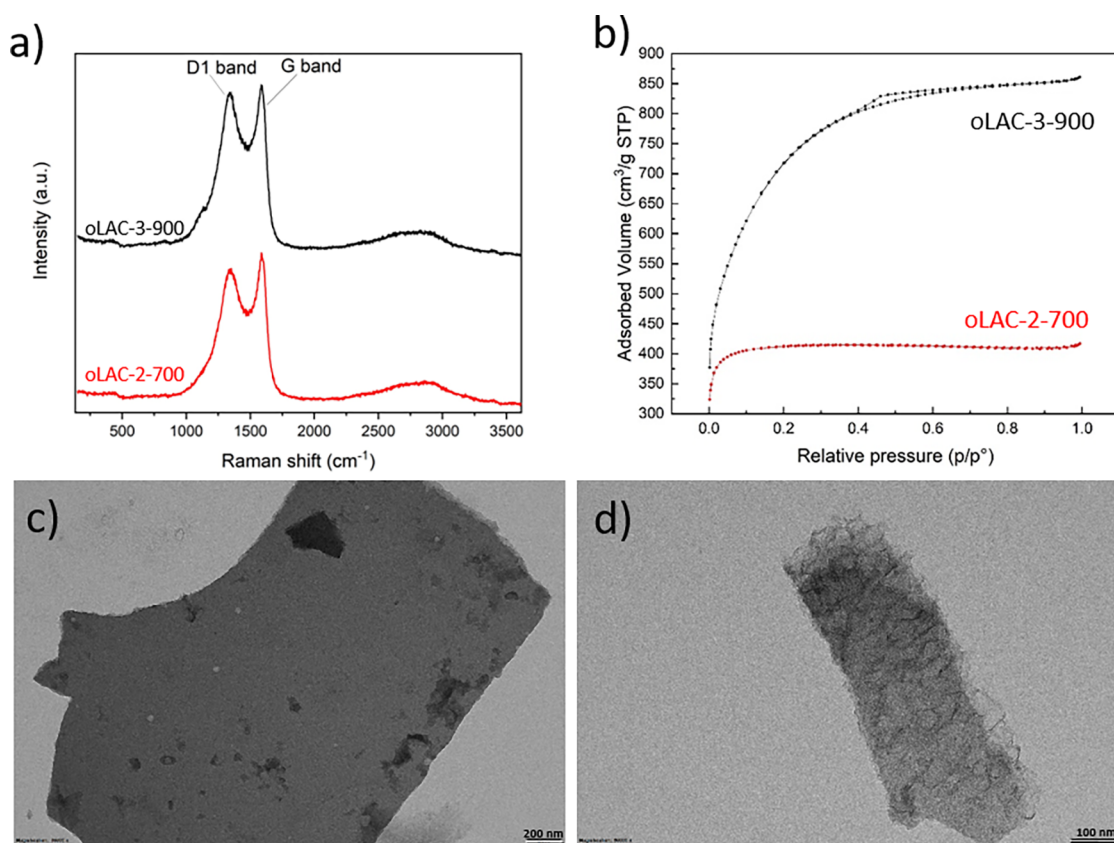
Figure 4. (a) Raman spectra of oLAC-2-700 (red) and oLAC-3-900 (black), (b) BET isotherms of oLAC-2-700 (red) and oLAC-3-900 (black), and representative TEM images of (c) oLAC-2-700 and (d) oLAC-3-900.

activity for the homocoupling reaction displayed by oLAC-3-800 and oLAC-3-900 (Figure 2a, green). We speculate that this effect can be ascribed to the bimolecular nature of the reaction, which needs a larger accessible surface to occur. Notably, the total oxygen content appears to be detrimental for the reaction (Figure 2b), although we hypothesize that O group distribution is the more decisive parameter affecting the catalytic activity, likely the ratio between carbonyls and acid groups, which has been previously identified as crucial in promoting homocoupling ODH reactions.[14,15] This trend is not observed in the case of THQ aromatization: in this case, the catalytic activity appears directly correlated with the oxygen content as well as the microporous volume (Figure 2c,d). The samples with the lowest amount of micropores (oLAC-3-900 and oLAC-3-800) are those with the lowest activity for the reaction (Figure 2c, orange). The reference test with GO (Table 1, entry 10) implies that the high O-content alone is not significantly affecting either of the reactions.

We have observed before that the quinone/carbonyl content in carbon materials is the driving force for high activity in these oxidative transformations. Moreover, we have observed how the carboxylic acid content affects differently each reaction, i.e., oxidative coupling seems to be more favored by highly acidic carbon materials (as GO and oAC$_{HNO3}$; see Table 1, entries 10 and 13) while THQ dehydrogenation does not benefit from this feature.[15] This behavior is recognizable in the different catalytic activities of highly acidic GO compared to rGO toward the examined reaction.

The relevance of carbonyl/quinone groups to the catalytic activity was evaluated by chemical blocking with 2,2,2-trifluoroethyl hydrazine[35] of the two most active materials

for the two reactions, and the labeled samples are referred to as oLAC-2-700 F-blocked and oLAC-3-900 F-blocked. The efficacy of the blocking protocol was evaluated by means of XPS analysis and is evidenced by the C−F peak visible at about 293 eV in the C1s spectrum as well as the peaks relative to N1s and F1s whose deconvolutions are reported in Figure S11. The O1s deconvoluted peak of the blocked material further supports the chemical change occurring on the surface of the material: the component associated with C=O groups (about 531.5 eV) is in fact significantly lowered when compared to the unmodified material (Figure 3). The residual C=O signals are due to C=O bonds other than ketonic carbonyls such as anhydrides, esters, and acids as well as to the fact that XPS is capable of probing 10−30 Å into the material,[36] reaching buried structural carbonyl groups that are accessible to molecular labeling and starting materials. When oLAC-2-700 F-blocked and oLAC-3-900 F-blocked were used as catalysts, yields of THQ aromatization and homocoupling dropped, respectively, to 14 and 9% (Table 1, entries 20 and 21), confirming the crucial role of these groups as active sites.

Raman spectroscopy (Figure 4a) of the two differently prepared activated carbons exhibits the typical D1 band around 1350 cm^{-1} of highly amorphous carbon materials. In addition, looking at the position and width of the G band, there must be a certain contribution of a secondary D2 band, around 1500 cm^{-1}, which is attributed to defects outside the planes of aromatic layers such as tetrahedral carbon in poorly organized materials.[37] A small shoulder around 1160 cm^{-1} can be seen, which is also characteristic of carbon materials with low crystallinity.[37] Overall, the two materials seem to present a similar amorphous character. As noted in the previous
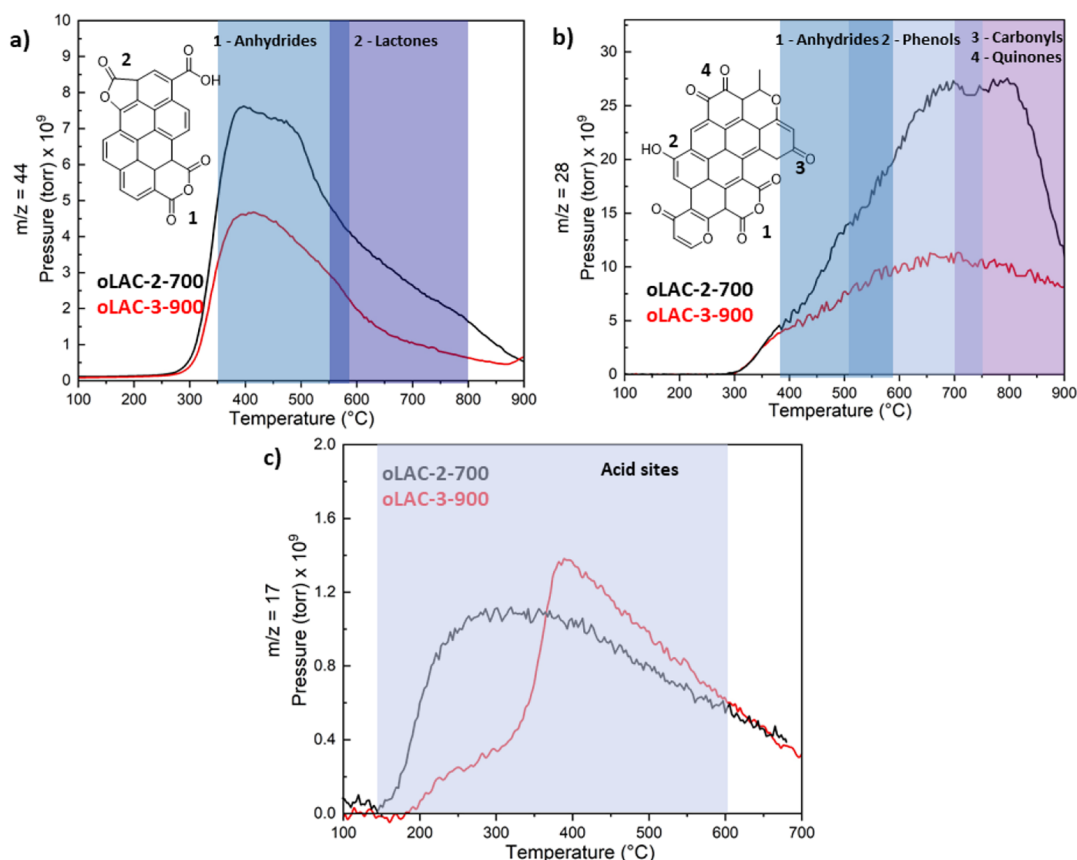
Figure 5. (a) CO_2 and (b) CO TPD profiles of desorption from the surface of pristine oLAC-2-700 (black) and oLAC-3-900 (red) after degassing at 300 °C, with marked regions of desorption temperatures and corresponding structures of oxygen functionalities, and (c) NH_3 desorption profile from oLAC-2-700 (black) and oLAC-3-900 (red) after NH_3 saturation at 110 °C for 60 min.

paragraph, the BET surface area and porosity vary greatly between samples prepared in different conditions, affecting the activity toward the different target reactions, and this is evidenced by the substantial difference between the two BET isotherms reported in Figure 3b: oLAC-2-700 is almost exclusively microporous and has a lower surface area, while the surface area is higher for oLAC-3-900, which presents also a relevant mesoporous content. Representative examples of TEM pictures are also shown in Figure 3c,d: both samples present themselves as flake-shaped structures; oLAC-3-900 exhibits overall smaller flakes, which look rougher and irregular compared to oLAC-2-700.

Inductively coupled plasma mass spectrometry (ICP-MS) was used to investigate the possible presence of residual metal impurities in oLAC-2-700 and oLAC-3-900. The study revealed that oLAC-3-900 contains a maximum of 1000 ppm level of Na as well as around 600 ppm K and Al, while other metals are present in very low amounts; oLAC-2-700 on the other hand contains <500 ppm K, and lower amounts of all the other metals that were investigated. As none of these metals are known to exhibit catalytic activity for the examined reactions, we confidently rule out any catalytic effect by metal impurities.

The acid−base properties were explored by temperature-programmed desorption (TPD) experiments under either NH_3 or CO_2 flow (see the Supporting Information). TPD of pristine materials shows evolution of CO and CO_2 for both materials, which starts at 300 °C, the temperature employed to pre-clean the samples. The CO and CO_2 bands have been analyzed using

literature values for temperature ranges at which specific functional groups desorb from carbon materials (Figure 5a,b).[6,15]

In good agreement with XPS data, oLAC-2-700 presents higher O-containing functional group loading; in particular, the area associated with CO evolution from decomposition of phenols, carbonyls, and quinones appears to be significantly more pronounced, compared to the same region for oLAC-3-900. At the same time, the NH_3 desorption curves after NH_3 saturation (Figure 5c) for the two materials appear very similar in intensity, suggesting a higher acid site relative abundance for oLAC-3-900. CO_2 desorption after saturation, on the other hand, shows no relevant basic sites on either material (see the Supporting Information).

The two different carbon materials were finally screened for catalytic activity in the two model reactions. It is known that the carbon materials' status as catalysts is controversial, and often there is a degree of stoichiometric behavior in oxidative processes. This feature has been recently accounted, in particular for some GO mediated reactions performed with over-stoichiometric "catalyst" loadings.[38] For this purpose, we carried out two experiments: (i) the reactions were run in the absence of the terminal oxidant O_2, under Ar; (ii) the catalyst was recycled up to four times to establish its robustness. For both reactions, the residual activity in the absence of oxygen is rather low, 32% compared to 65% in the presence of O_2 for the homocoupling with oLAC-3-900 and 26% compared to 60% for the aromatization with oLAC-2-700. We interpret it as evidence that the studied ODH reactions are unlikely to be
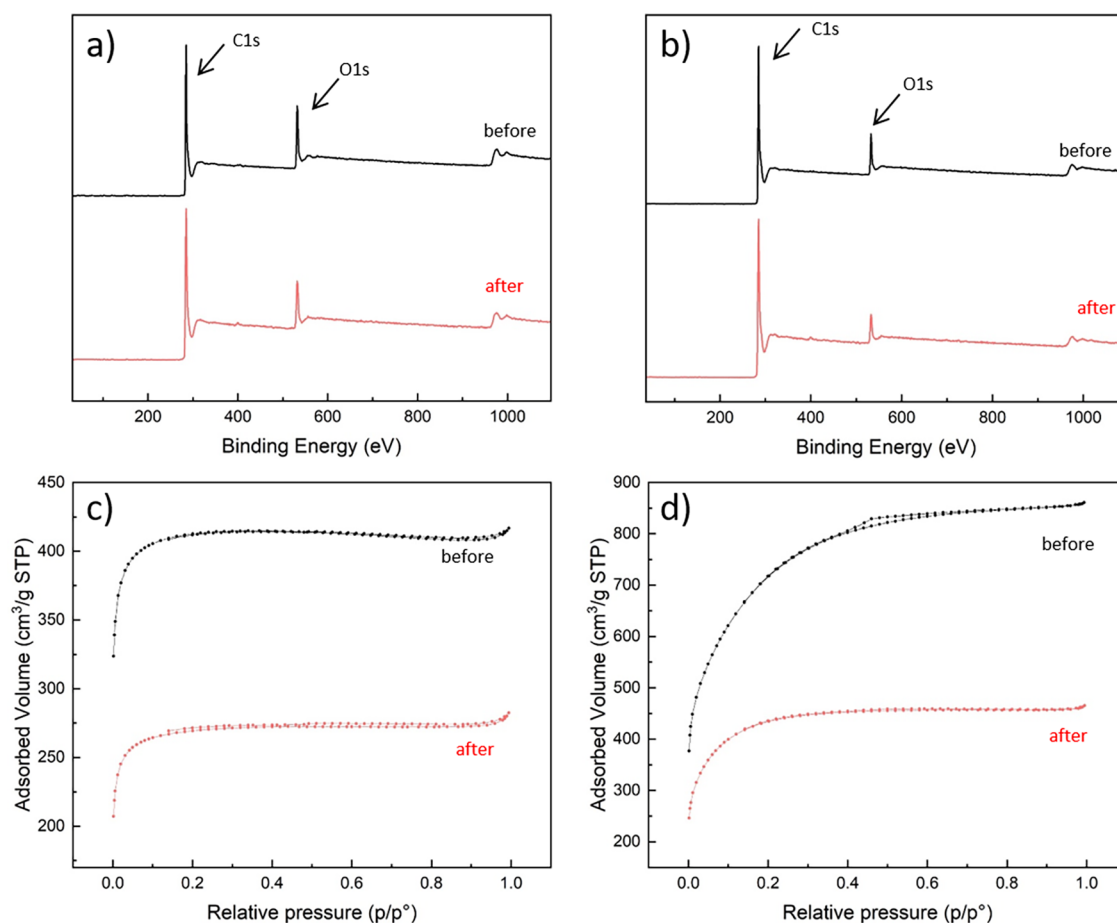
Figure 6. XPS survey spectra of (a) oLAC-2-700 and (b) oLAC-3-900 before (black) and after (red) catalysis and BET isotherms of (c) oLAC-2-700 and (d) oLAC-3-900 before (black) and after (red) catalysis.

mediated via activated dioxygen (superoxides),[39] while the residual activity suggests at least partial catalytic behavior for the material. The reactions were also performed in the presence of stoichiometric amounts of butylated hydroxytoluene (BHT), a typical quencher of superoxide and hydroperoxyl radicals. No noticeable decrease in catalytic activity was observed, indicating that oxygen radicals are not responsible for the promotion of the oxidative process.

As carbon materials have been previously reported to promote the acceptorless dehydrogenation of THQ,[40] the performance of oLAC-2-700 in the absence of O_2 was further explored by evaluating its capability for hydrogen production: the reaction was run under Ar flow and the evolved gases were analyzed via an in-line gas chromatographer. H_2 formed for the initial 15 min with a relatively high rate of 3.8 mmol h^{-1} g_{cat}^{-1}. However, after this initial time, no more hydrogen evolved, suggesting that the reaction rapidly deactivates in the absence of electron donors such as O_2. The kinetics of THQ dehydrogenation in Ar were also studied (Figure S14) and revealed that the observed activity is restricted to the first 30 min of reaction time. This suggests that both effects are correlated with the stoichiometric component of the material's activity.

An additional test was run under an Ar atmosphere adding 1 equiv of hydrogen peroxide, which resulted in slightly higher yields of 36 and 39%, respectively, for the homocoupling and the aromatization at the expense of reaction selectivity as unidentified side products have been detected via NMR.

Concerning the recycling experiments, in the case of THQ aromatization, the activity was satisfactorily maintained during the first recycling, where it decreased only from 60 to 55%, with an overall loss of 20% over four cycles. However, for the homocoupling reaction, a significant loss of activity was observed after the first cycle, where yield drops from 65 to 23%, revealing a possible partial stoichiometric reaction with the strongly nucleophilic substrate, which was already hypothesized in a previously analyzed case.[14] XPS analysis of the recycled catalysts revealed a significant loss of oxygen content after the first cycle for both materials from 10 to 7% for oLAC-3-900 and from 15 to 11% for oLAC-2-700, together with the formation of a nitrogen peak, suggesting possible partial stoichiometric reactivity of THQ with the catalytically active sites (Figure 6). Unfortunately, we failed to restore the original activity by any chemical washing, not even with an additional nitric acid or thermal treatment. Additionally, BET analysis revealed a dramatic decrease in surface area, evidencing the impactful effect of the reaction conditions on the materials' structural properties. It is worth noting that oLAC-3-900 loses most of its mesoporosity, retaining almost only the micropores, while oLAC-2-700 loses almost half of its microporous volume. Hence, it seems that in comparison to previously reported oxidized commercial activated carbon, there is some tradeoff of high catalytic activity with material fragility.
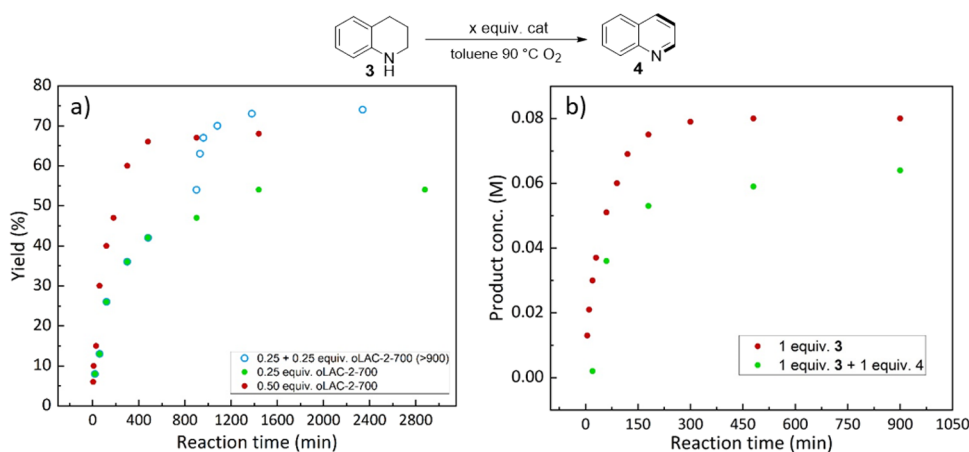
Figure 7. Reaction monitoring over time for the dehydrogenation of THQ **3** using oLAC-2-700 as the catalyst (a) with different catalyst loadings, 0.50 equiv (red circles), 0.25 equiv (green circles), and 0.25 + 0.25 added after 900 min (blue hollow circles) and (b) with different initial substrate and product concentrations, 1 equiv **3** (red circles) and 1 equiv **3** + 1 equiv **4** (green circles). Catalyst loading defined as 1 equiv = 224 mg/mmol, in line with our previous work.[14]

Next, we performed additional kinetic experiments to study the effect of catalyst loading and evaluate product inhibition contribution to the catalytic activity.

We measured the conversion profiles for THQ **3** dehydrogenation with varying loadings of oLAC-2-700 and different initial concentrations for the substrate (**3**) and product (**4**), see Figure 7. First, we performed the reaction using 0.25 equiv of catalyst loading and 1 equiv of the starting material (starting concentration, 0.1 M): in such conditions, the product concentration reached a plateau at 53 mM (54% yield) (Figure 7a, solid green circles). By doubling the catalyst loading (Figure 7a, solid red circles), the maximum concentration reached was 67 mM (yield improved by 13%) and the reaction exhibited a higher rate of conversion. To assess the stoichiometric component of the catalysis, we ran the reaction with 0.25 equiv of catalyst loading for 930 min, *i.e.*, until the product concentration reached a plateau and then added a second 0.25 equiv of the catalyst (Figure 6a, hollow blue circles). Interestingly, the reaction produced only 6% overall higher yield (72 mM product) compared to the one starting with 0.5 equiv of the catalyst.

We then varied the initial substrate and product concentrations while using a higher 1 equiv loading of oLAC-2-700, see Figure 7b. When running the reaction with 1 equiv of the starting material **3** and catalyst, the product concentration plateaued at 80 mM (80% yield) (Figure 7b, solid red circles). However, the reaction run with 1 equiv of substrate **3**, product **4**, and catalyst as the initial amounts, to determine catalyst inhibition, was significantly slower: the product concentration (subtracting the initially added 0.1 M) reached its maximum at 64 mM (64% yield) after 900 min (Figure 7b, solid green circles). This indicates that product inhibition is occurring during the reaction. This effect could be due to the strong physisorption of the aromatic product on the carbon surface, which inhibits the catalytic sites, this requiring implementation of a separation protocol that will have to be considered in future catalysis developments. Simple catalyst filtration/washing could represent a feasible strategy to remove all the physisorbed product from the catalyst surface, while the use of flow reactors could significantly improve the turnover frequencies.

To evaluate the extent of the possible applications for these carbons, we selected some cutting-edge carbocatalyzed OHD reactions recently reported in literature (Figure 8).
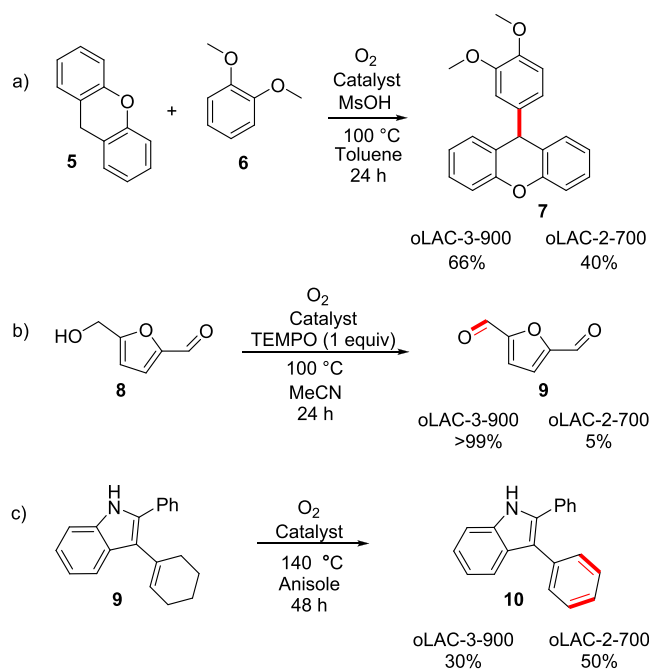

Figure 8. Testing of oLAC-3-900 and oLAC-2-700 in selected carbocatalyzed OHD reactions: (a) C−C heterocoupling of xanthene and veratrole, (b) 5-hydroxymethylfurfural oxidation, and (c) aromatization of 2-phenyl-3-(cyclohexenyl)-indole.

Originally, Loh and co-workers developed GO and MsOH catalyzed cross-coupling of xanthene (**5**) with veratrole (**6**), for which quinone and zigzag edges of the carbon material were suggested as active sites (Figure 7).[41] Our experiments with lignin-derived carbons under similar conditions delivered fruitfully the coupling product **7** but with slightly lower yields compared to the originally reported 75%. Interestingly, we observed different activities for the carbocatalysts tested, with oLAC-3-900 outperforming oLAC-2-700, as it did in the homocoupling tested before. As a second reference reaction,
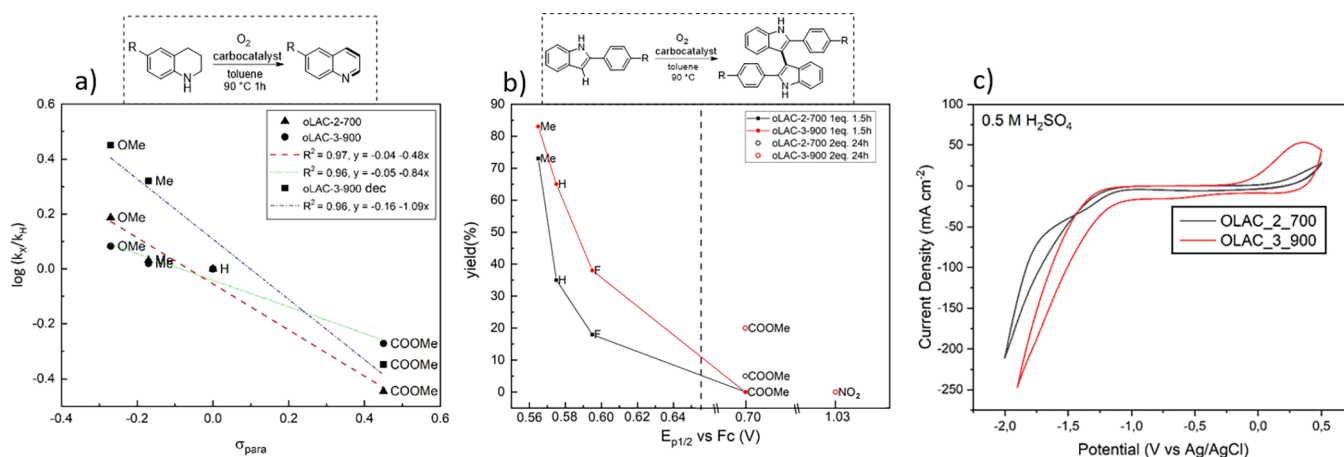
Figure 9. (a) Hammett plot for the aromatization of 6-R-THQs with oLAC-2-700 (triangles), oLAC-3-900 (circles), and oLAC-3-900 decarboxylated (squares); (b) experimental oxidation potential yield correlation for the homocoupling of differently substituted indoles with oLAC-2-700 (black) and oLAC-3-900 (red); (c) cyclic voltammetry of oLAC-2-700 (black) and oLAC-3-900 (red) in H_2SO_4 0.5 M.

we selected 5-hydroxymethylfurfural (**8**) oxidation to 2,5-diformylfuran (**9**), which is a crucial process for the valorization of a renewable feedstock chemical. Hou and co-workers exposed that, even though this reaction is sluggish with GO, in the presence of TEMPO as the co-catalyst, high conversion can be achieved.[42] Equally high activities were observed for oLAC-3-900 in the same conditions with over 99% conversion in 24 h. The reaction did not proceed at all, anyway, in the presence of oLAC-2-700, confirming the very different catalytic activities of the two materials. As the alcohol oxidation is mediated by the nitrosonium cation of TEMPO,[43] oLAC-3-900 generates this species more swiftly, indicating that the catalyst is a better electron oxidant. As a third reference reaction, we explored the aromatization of 2-phenyl-3-(cyclo-hexenyl)-indole (**9**) to the corresponding 2,3-diphenylindole (**10**). This reaction was developed in our recent study[15] using commercially available oxidized activated carbon as the catalyst. Under the same conditions, oLAC-3-900 oxidized indole derivatives **9** to **10** with a modest 30% yield, but oLAC-2-700 allowed us to obtain **10** in 50%, proving to be the best catalyst for aromatization processes. The above diverse ODH reactivity indicates that lignin-derived active carbons have potential for wide applicability to mediate organic ODH transformations.

From these experiments and previous observations, it appears that the catalysts prepared have different preferred mechanisms of action. According to our previous studies, the bimolecular indole homocoupling proceeds via single-electron transfer (SET) mediated catalysis, whereas OHD aromatization of 1,2,3,4-tetrahydroquinoline to quinoline is a unimolecular reaction, for which hydride abstraction has been proposed to be the rate-limiting step (Scheme 1). On one hand, oLAC-2-700 seems to favor aromatization reactions, which have been proposed to proceed via hydride abstraction by the catalyst. On the other hand, oLAC-3-900, which is more efficient in mediating the couplings and oxidizing TEMPO, operates preferentially via SET.

The hypothesized hydride abstraction during THQ aromatization, with the possible association of a positive charge with the transition state of the rate-limiting step, was probed, by constructing the Hammett plot, a method to describe how the meta- or para-phenyl substituents influence the activity of the substrates related to reaction rates.

According to this model, different reactions will exhibit different influences, which are related to the charging state of intermediates.[15,17] The reaction was run for 60 min with THQs bearing different substituents at the 6-position, with the two different catalysts. The observed negative ρ values obtained for both catalysts support our hypothesis (Figure 9a); however, the entity of the substituent effect seems to be different for the different catalysts. We associated the lower ρ value (−0.48) for oLAC-3-900 with the increased acidity of the material, which generally slows down the reaction by H-bonding THQ, making the effect less dramatic. This hypothesis was further substantiated by performing the same study with oLAC-3-900 after acid groups were removed through a decarboxylating treatment described in our previous paper (oLAC-3-900 dec).[15] As anticipated, the decarboxylated catalyst shows an even more negative ρ value (−1.09) and faster reaction rates, supporting our hypothesis.

Our previous aryl homocoupling studies with different carbon materials (oAC and oCNT) indicate that the reactivity of the substrates correlates with their oxidation potential. Herein, we used a set of differently substituted indoles exhibiting different oxidation potentials according to our electrochemical measurements (see the Supporting Information) to examine whether different carbon materials could have different oxidation abilities. Homocoupling experiments were run with indoles substituted at the *para* position of the phenyl ring. The correlation between the reaction rate and the measured oxidation potential of the different indoles is shown in Figure 9b. For 2-(4-methylphenyl), 2-phenylindole, and 2-(4-fluorophenyl)indole, there is an almost linear correlation between yield and oxidation potential (83−18%, 0.565−0.595 V vs Fc), while an abrupt loss of activity is observed in the same reaction conditions (1 equiv catalyst and 1.5 h reaction time) when moving to methyl 4-(indol-2-yl)benzoate, in which oxidation potential is significantly higher (0.7 V vs Fc). Doubling the catalyst loading and running the reaction for 24 h, it is possible to observe the formation of some product; however, the same conditions are not sufficient to couple 2-(4-nitrophenyl)indole. We reason that this indole's oxidation potential (1.03 V vs Fc) is way too high compared to the carbocatalysts we used, so the SET needed to start the coupling reaction is not happening. Although for both catalysts this seems to be the limit, the systematically better activity of
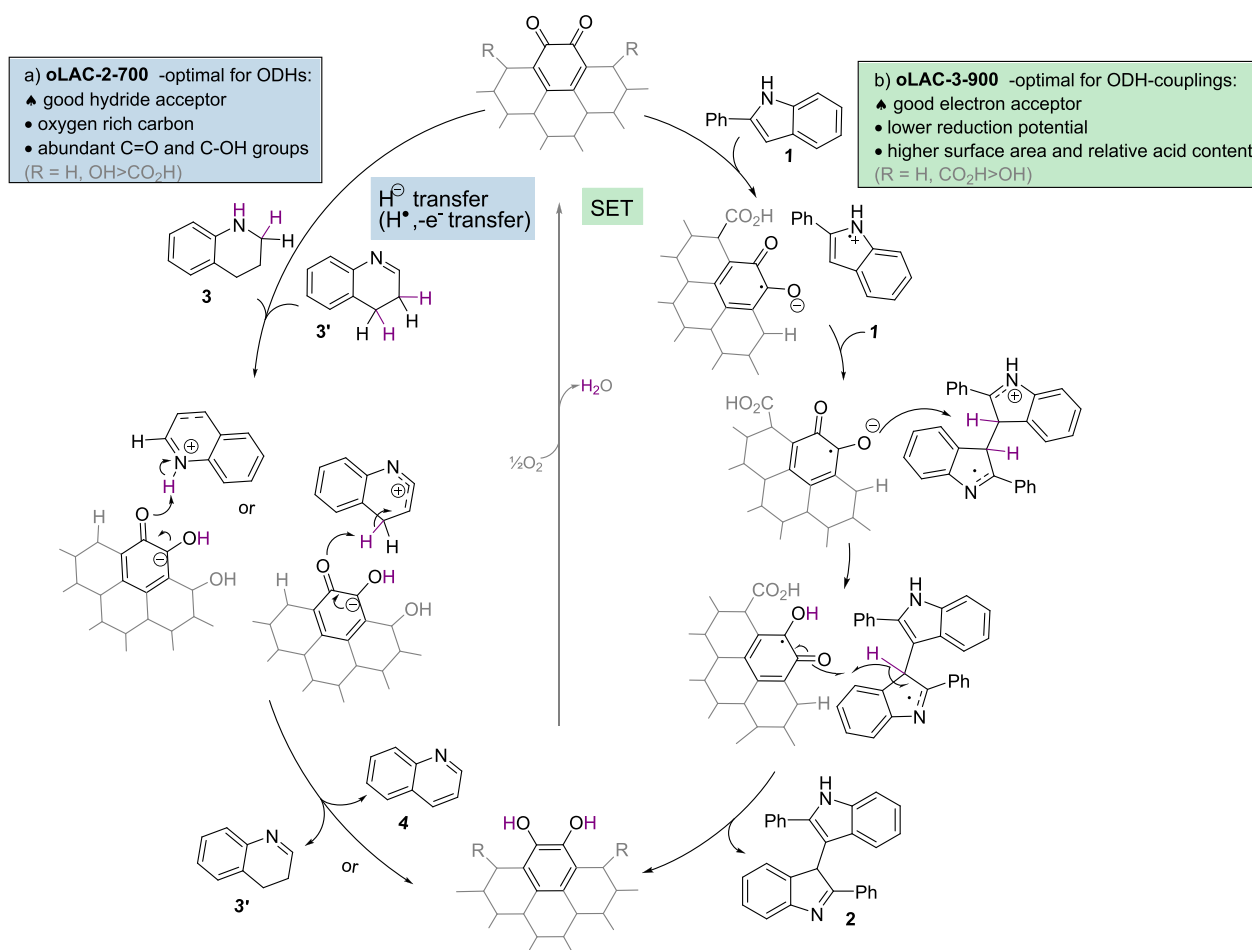
Figure 10. Proposed mechanistic pathways for the probe reactions with (a) oLAC-2-700 and (b) oLAC-3-900 as catalysts.

oLAC-3-900 suggests that its reduction potential is slightly higher than the one of oLAC-2-700. This hypothesis is further corroborated by electrochemical characterization of the catalysts: oLAC-700 and oLAC-900 were measured by means of cyclic voltammetry using a Toray paper supporting working electrode (Figure 8c). From the comparison of the voltammetric curves, both materials are clearly active toward H_2 evolution (HER) with an onset potential at −1.2 V (vs Ag/AgCl). The significantly increased current density shown by oLAC-900, though, is an indication of its improved electron transfer ability, supporting the SET route as its preferential mechanistic pathway. These considerations suggest that it is possible to tune the catalytic properties, including the activity toward a specific catalytic mechanism by changing the preparation parameters of carbon materials from biomass.

To summarize the characteristic catalyst properties and their operation with the model reactions, we suggest that both oLAC-2-700 and oLAC-3-900 operate via a quinoidic mechanism with some distinct features (Figure 10). The oLAC-2-700 is a better hydride acceptor simply due to the high loading of oxygen, with functional groups, including the active quinones, and possible assisting groups such as phenols, in abundance and more even distribution as observed via XPS and TPD. For oLAC-3-900, we consider that the coupling reaction is favored by both the high surface area and the lower reduction potential, granted by the relative abundance of acid sites determined by TPD, which are known to promote this reaction.[14,15] The latter enables the smooth electron transfer

reaction to 2-phenylindole (**1**), while the former may stabilize coupling reaction radical intermediates.

■ CONCLUSIONS

We have developed protocols to convert spruce organosolv lignin into catalytically active material for OHD reactions. The enhanced catalytic activity outperforming both oxidized commercial active carbons and other common carbocatalysts like GO is associated with the structural and surface properties, and their application has the potential to be extended to a wide range of organic oxidative transformations. Morphologic features and oxygen content can be tailored by choosing the right activation parameters, mainly the KOH:lignin ratio and temperature and by diluted HNO_3 oxidation.

A high oxygen content, in particular C═O/C─OH groups, combined with a large microporous volume, is beneficial for dehydrogenative aromatization reactions involving hydrogen atoms or hydride transfer, whereas one-electron oxidation mediated couplings and reactions are better catalyzed by carbon material with a higher external surface area and relative abundance of acid sites, even if the oxygen content is lower. The material developed shows high activity despite its low degree of oxidation compared to other oxidized carbon materials commonly used as catalysts, like GO,[44] suggesting that the tailoring of morphologic properties of activated carbon materials can be crucial in determining their catalytic activity as much as their oxygen content. Future developments are needed to improve the recyclability of materials and reduce

their partial reagent nature. Based on the observations, we envision that the preparation protocol should be further developed to increase the graphitic character of lignin-derived materials as their highly amorphous nature could be lowering their physico-chemical stability, making them less durable. The challenging part would be achieving such properties without sacrificing the surface area and oxygen content, which are crucial features for catalytic activity toward the studied reactions. Overall, the developed preparation protocols and reported catalytic performance demonstrate how lignin, a common industrial side product with limited intrinsic value, can constitute a promising raw material for the preparation of functional carbon materials.

■ MATERIALS AND METHODS

General Remarks. All reagents were commercially available and used without further purification as obtained from the supplier. All oxidized active carbon species (oAC) were synthesized in our lab. All HPLC-grade solvents were used without further purification as obtained from the supplier (Honeywell, VWR, Merck, Sigma-Aldrich). Distilled water was produced with an Aquatron AS4 (Bibby). All NMR spectra were measured at a sample temperature of 293 K. The following device was used: Avance Neo 500 (Bruker, 500 MHz). The spectra were calibrated to the residual proton shifts of the corresponding deuterated solvents (^{1}H NMR: CDCl$_3$ 7.26 ppm, DMSO-d_6: 2.50 ppm). NMR yields were determined with 1,3,5-trimethoxybenzene as an internal standard using a pulse width of pw = 3.33 μs and a delay time of d1 = 35 s.

Catalyst Preparation. Detailed characterization of spruce organosolv lignin was reported earlier.[45] Lignin (2 g) was stirred with 2, 4, or 6 g of KOH in ca. 50 mL of water for 1 h, and the water was then evaporated at 110 °C and then dried under vacuum overnight. The impregnated lignin was then grinded and transferred to a crucible and pyrolyzed in an oven for 3 h at 700, 800, or 900 °C with a temperature ramp of 5 °C/min under an Ar atmosphere (flow of around 50 mL/min). The carbonized solid obtained was grinded, neutralized with HCl (conc.), and washed with water on Büchner until the filtrate was neutral. The carbon material was then dried on a vacuum pump, transferred in a flask, and left to dry in air overnight. A portion of each sample was oxidized with diluted nitric acid. Carbon material (100−150 mg) was dispersed in a 4 M HNO$_3$ solution to obtain a suspension of 1 mg/mL. The mixture was sonicated for 15 min and left stirring for 3 h. The solid was then filtered on Büchner and washed with ion-exchanged water until the filtrate was neutral. The carbon material was then dried on a vacuum pump, transferred in a flask, and left to dry in air overnight. Every subsequent batch was tested for repeatability by running the studied reactions in standard conditions.

Characterization. The X-ray photoelectron spectroscopy (XPS) analysis was performed by a Thermo Fisher Scientific ESCALAB 250Xi XPS system at the Center of Microscopy and Nanotechnology, University of Oulu (Finland). The monochromatic AlKα radiation (1486.7 eV) operated at 20 mA and 15 kV. The powder samples were put in a gold sample holder, and O, C, N, and Au were measured for all samples. The measurement data were analyzed by the Avantage V5 program developed by Thermo Fisher Scientific. Charge compensation was used to determine the presented spectra, and the binding energies (BEs) were calibrated by a C1s peak position of 284.8

eV. Raman spectra were recorded on a NT-MDT Ntegra confocal Raman microscope using an excitation wavelength of 532 nm, output power of 22 mW, and an ND1 filter. Preparation of the samples was carried out via deposition of the powder onto silicon wafers. For each sample, three points were recorded in back scattering mode and averaged. N$_2$ physisorption experiments were performed with a Micrometrics ASAP 2020 automatic analyzer. The samples were first degassed under vacuum at 120 °C for 12 h before the N$_2$ adsorption at liquid nitrogen temperature. The microporous volume and microporous surface area were determined by the analysis of the t-plot of the corresponding isotherms. TEM images were collected with a TEM Philips EM208 using an acceleration voltage of 100 kV. Samples were dispersed in ethanol and drop-cast onto a TEM grid (200 mesh, copper, carbon only).

Catalytic Testing. The setup for both standard reactions was as follows: 0.1 mmol of the starting material and carbocatalyst (224 mg/mmol) were weighted into a 5 mL Biotage microwave vial, and 1 mL of toluene was added (Table 2). The vial was sealed with the appropriate septum cap to make it air-tight. The mixture was saturated with O$_2$ by three successive vacuum-O$_2$ cycles and left stirring at 90 °C in an O$_2$ atmosphere for the necessary time (generally 1.5 h). The reference test under Ar was set up with the same procedure. The mixture was then filtered through Celite and washed with ca. 50 mL of DCM. The solvents were removed, and the crude mixture was dissolved in 1 mL of DMSO-d_6 and analyzed with ^{1}H NMR (500 MHz, DMSO) in the presence of a capillary tube filled with a solution of 1,3,5-trimethoxybenzene in a known concentration as the internal standard to determine the yield of the reaction. The reported yields were obtained by the average of two catalytic tests. Kinetic experiments were carried out the same way by stopping the reaction and working it up at each required reaction time. All yields were NMR yields.

Oxygen-Free Catalytic Experiments: H$_2$ Evolution Evaluation. The catalyst (100 mg) was dispersed into 5 mL of toluene in a two-neck flask with silicon septa and degassed by flowing argon for 1 h while heating the mixture at 90 °C. The flask was then left to cool down, and tetrahydroquinoline (0.5 mmol) was added with a syringe under Ar flow. One of the two necks of the flask was connected to gas chromatography (Agilent 8860). The mixture was heated again at 90 °C, and the evolution of H$_2$ was detected using a gas chromatography detector (TCD) by automatic sampling of the reactor head space every 15 min.

Derivatization of oLAC-1-700 and oLAC-3-900 with 2,2,2-Trifluoroethyl Hydrazine. Carbon material (50 mg) was put in a small vial and inserted in a Schlenk flask where 250 μL of 2,2,2-trifluoroethyl hydrazine was injected. The flask was frozen with liquid N$_2$, and vacuum was used for 5 min. The flask was then left to warm up to room temperature under vacuum for 3 days.[14]

Degassing of oLAC-2-700. Carbon material (20 mg) was put in a vial and heated at 100 °C under vacuum for 16 h.

Recyclability Tests. As described before, for the standard setup, 0.4 mmol of the starting material and 90 mg of the carbocatalyst were mixed in 4 mL of toluene. After a 1.5 h reaction mixture was filtered through filter paper in a Büchner-like filtration with a round bottomed flask and a funnel, DCM (approximately 200 mL) was used to rinse products from the carbon. DCM was evaporated under reduced pressure, and the yield was calculated by NMR as described before. Filtered

carbons were dried under vacuum for 2 h and then in air overnight before reuse.

■ ASSOCIATED CONTENT

ⓢ Supporting Information

The Supporting Information is available free of charge at https://pubs.acs.org/doi/10.1021/acscatal.3c02735.

> Experimental details, additional BET, TPD, NMR and XPS spectra, ICP-MS data, and electrochemical measurements (PDF)

■ AUTHOR INFORMATION

Corresponding Author

Juho Helaja − *Department of Chemistry, University of Helsinki, 00014 Helsinki, Finland;* ⓞ orcid.org/0000-0001-8645-617X; Email: juho.helaja@helsinki.fi

Authors

Anna Lenarda − *Department of Chemistry, University of Helsinki, 00014 Helsinki, Finland*

Michele Melchionna − *Department of Chemical and Pharmaceutical Sciences, INSTM, University of Trieste, 34127 Trieste, Italy;* ⓞ orcid.org/0000-0001-9813-9753

Santeri Aikonen − *Department of Chemistry, University of Helsinki, 00014 Helsinki, Finland*

Tiziano Montini − *Department of Chemical and Pharmaceutical Sciences, INSTM, University of Trieste, 34127 Trieste, Italy;* ⓞ orcid.org/0000-0001-9515-566X

Paolo Fornasiero − *Department of Chemical and Pharmaceutical Sciences, INSTM, University of Trieste, 34127 Trieste, Italy;* ⓞ orcid.org/0000-0003-1082-9157

Tao Hu − *Research Unit of Sustainable Chemistry, University of Oulu, 90570 Oulu, Finland*

Michael Hummel − *Department of Bioproducts and Biosystems, Aalto University, 02150 Espoo, Finland;* ⓞ orcid.org/0000-0002-6982-031X

Complete contact information is available at:
https://pubs.acs.org/10.1021/acscatal.3c02735

Author Contributions

A.L.: method and catalyst development, catalyst testing, analysis of results, and writing-original draft; M.M.: BET analysis, electrochemical characterization, and H_2 evolution experiments; S.A.: analysis of kinetic data and editing; T.M. and P.F.: TPD experiments and interpretation; T.H.: XPS characterization and ICP-MS characterization; M.H.: writing-editing and funding acquisition; J.H.: supervision, writing-editing, project administration, and funding acquisition.

Notes

The authors declare no competing financial interest.

■ ACKNOWLEDGMENTS

■ REFERENCES

(1) (a) Su, D. S.; Zhang, J.; Frank, B.; Thomas, A.; Wang, X.; Paraknowitsch, J.; Schlögl, R. Metal-free heterogeneous catalysis for sustainable chemistry. *ChemSusChem* 2010, 3, 169−180. (b) Chua, C. K.; Pumera, M. Carbocatalysis: The state of "metal-free" catalysis. *Chem. − Eur. J.* 2015, 21, 12550−12562.

(2) (a) Su, D. S.; Wen, G.; Wu, S.; Peng, F.; Schlögl, R. Carbocatalysis in liquid-phase reactions. *Angew. Chem., Int. Ed.* 2017, 56, 936−964. (b) Lenarda, A.; Wirtanen, T.; Helaja, J. Carbon materials as catalytic tools for oxidative dehydrogenations and couplings in liquid phase. *Synthesis* 2023, 55, 45−61.

(3) Dreyer, D. R.; Bielawski, C. W. Carbocatalysis: Heterogeneous carbons finding utility in synthetic chemistry. *Chem. Sci.* 2011, 2, 1233−1240.

(4) (a) Su, D. S.; Perathoner, S.; Centi, G. Nanocarbons for the development of advanced catalysts. *Chem. Rev.* 2013, 113, 5782−5816. (b) Jung, H.; Bielawski, C. W. Soluble asphaltene oxide: A homogeneous carbocatalyst that promotes synthetic transformations. *RSC Adv.* 2020, 10, 15598−15603. (c) Jung, H.; Bielawski, C. W. Asphaltene oxide promotes a broad range of synthetic transformations. *Chem. Commun.* 2019, 2, 113.

(5) (a) Navalon, S.; Dhakshinamoorthy, A.; Alvaro, M.; Antonietti, M.; García, H. Active sites on graphene-based materials as metal-free catalysts. *Chem. Soc. Rev.* 2017, 46, 4501−4529. (b) Antonietti, M.; Lopez-Salas, N.; Primo, A. Adjusting the structure and electronic properties of carbons for metal-free carbocatalysis of organic transformations. *Adv. Mater.* 2019, 31, No. e1805719.

(6) (a) Figueiredo, J. L.; Pereira, M. F. R. The role of surface chemistry in catalysis with carbons. *Catal. Today* 2010, 150, 2−7. (b) Figueiredo, J. L.; Pereira, M. F. R.; Freitas, M. M. A.; Órfão, J. J. M. Modification of the surface chemistry of activated carbons. *Carbon* 1999, 37, 1379−1389.

(7) Qi, W.; Liu, W.; Zhang, B.; Gu, X.; Guo, X.; Su, D. Oxidative dehydrogenation on nanocarbon: Identification and quantification of active sites by chemical titration. *Angew. Chem., Int. Ed.* 2013, 52, 14224−14228.

(8) Qi, W.; Su, D. Metal-Free carbon catalysts for oxidative dehydrogenation reactions. *ACS Catal.* 2014, 4, 3212−3218.

(9) (a) Dreyer, D. R.; Todd, A. D.; Bielawski, C. W. Harnessing the chemistry of graphene oxide. *Chem. Soc. Rev.* 2014, 43, 5288−5301. (b) Jia, H.-P.; Dreyer, D. R.; Bielawski, C. W. C−H oxidation using graphite oxide. *Tetrahedron* 2011, 67, 4431−4434. (c) Morimoto, N.; Suzuki, H.; Takeuchi, Y.; Kawaguchi, S.; Kunisu, M.; Bielawski, C. W.; Nishina, Y. Real-time, in situ monitoring of the oxidation of graphite: Lessons learned. *Chem. Mater.* 2017, 29, 2150−2156.

(10) (a) Zaytseva, O.; Neumann, G. Carbon nanomaterials: production, impact on plant development, agricultural and environmental applications. *Chem. Biol. Technol. Agric.* 2016, 3, 17. (b) Fadeel, B.; Bussy, C.; Merino, S.; Vázquez, E.; Flahaut, E.; Mouchet, F.; Evariste, L.; Gauthier, L.; Koivisto, A. J.; Vogel, U.; Martín, C.; Delogu, L. G.; Buerki-Thurnherr, T.; Wick, P.; Beloin-Saint-Pierre, D.; Hischier, R.; Pelin, M.; Candotto Carniel, F.; Tretiach, M.; Cesca, F.; Benfenati, F.; Scaini, D.; Ballerini, L.; Kostarelos, K.; Prato, M.; Bianco, A. Safety assessment of graphene-based materials: Focus on human health and the environment. *ACS Nano* 2018, 12, 10582−10620.

(11) (a) Schaetz, A.; Zeltner, M.; Stark, W. J. Carbon modifications and surfaces for catalytic organic transformations. *ACS Catal.* 2012, 2, 1267−1284. (b) Serp, P.; Corrias, M.; Kalck, P. Carbon nanotubes and nanofibers in catalysis. *Appl. Catal., A* 2003, 253, 337−358.

(12) (a) Guerrero-Ruiz, A.; Rodríguez-Ramos, I. Oxydehydrogenation of ethylbenzene to styrene catalyzed by graphites and activated carbons. *Carbon* 1994, 32, 23−29. (b) Gniot, I.; Kirszensztejn, P.; Kozłowski, M. Oxidative dehydrogenation of isobutane using modified activated carbons as catalysts. *Appl. Catal., A* 2009, 362, 67−74.

(13) Hayashi, M. Oxidation using activated carbon and molecular oxygen system. *Chem. Rec.* 2008, 8, 252−267.

(14) Wirtanen, T.; Mäkelä, M. K.; Sarfraz, J.; Ihalainen, P.; Hietala, S.; Melchionna, M.; Helaja, J. Carbocatalysed oxidative C_{sp}^2-C_{sp}^2 homocouplings of benzo-fused heterocycles. *Adv. Synth. Catal.* 2015, 357, 3718−3726.

(15) Enders, L.; Casadio, D. S.; Aikonen, S.; Lenarda, A.; Wirtanen, T.; Hu, T.; Hietala, S.; Ribeiro, L. S.; Pereira, M. F. R.; Helaja, J. Air oxidized activated carbon catalyst for aerobic oxidative aromatizations of N-heterocycles. *Catal. Sci. Technol.* **2021**, *11*, 5962–5972.

(16) Mäkelä, M. K.; Bulatov, E.; Malinen, K.; Talvitie, J.; Nieger, M.; Melchionna, M.; Lenarda, A.; Hu, T.; Wirtanen, T.; Helaja, J. Carbocatalytic cascade synthesis of polysubstituted quinolines from aldehydes and 2-vinyl anilines. *Adv. Synth. Catal.* **2021**, *363*, 3775–3782.

(17) Yang, M.; Lenarda, A.; Frindy, S.; Sang, Y.; Oksanen, V.; Bolognani, A.; Hendrickx, L.; Helaja, J.; Li, Y. A metal-free carbon catalyst for oxidative dehydrogenation of aryl cyclohexenes to produce biaryl compounds. *PNAS* **2023**, *120*, No. e2303564120.

(18) Marsh, H.; Rodríguez-Reinoso, F. *Activated carbon*; Elsevier, Amsterdam, 2006 pp. 3–6.

(19) (a) Sircar, S.; Golden, T. C.; Rao, M. B. Activated carbon for gas separation and storage. Carbon 1996, 34 (1), 1–12. DOI: 10.1016/0008-6223(95)00128-X; (b) Pui, W. K.; Yusoff, R.; Aroua, M. K. A review on activated carbon adsorption for volatile organic compounds (VOCs). *Rev. Chem. Eng.* **2019**, *35*, 649–668. (c) Jjagwe, J.; Olupot, P. W.; Menya, E.; Kalibbala, H. M. Synthesis and application of granular activated carbon from biomass waste materials for water treatment: A review. *J. Bioresour. Bioprod.* **2021**, *6*, 292–322.

(20) Pereira, M. F. R.; Órfão, J. J. M.; Figueiredo, J. L. Oxidative dehydrogenation of ethylbenzene on activated carbon fibers. *Carbon* **2002**, *40*, 2393–2401.

(21) (a) Melchionna, M.; Fornasiero, P.; Prato, M. Into the carbon: A matter of core and shell in advanced electrocatalysis. *APL Mater.* **2020**, *8*, 20905. (b) Kiciński, W.; Dyjak, S. Transition metal impurities in carbon-based materials: Pitfalls, artifacts and deleterious effects. *Carbon* **2020**, *168*, 748–845.

(22) Tour, J. M. Top-Down versus Bottom-Up Fabrication of Graphene-Based Electronics. *Chem. Mater.* **2014**, *26*, 163–171.

(23) Wu, S.; Pan, X.; Xu, S.; Lin, Y.; Yan, H.; Wen, G.; Diao, J.; Liu, H. A facile strategy based on the metal-free design of carbon to deliver an insight into the active sites for liquid phase carbocatalysis. *Chem. Commun.* **2020**, *56*, 3789–3792.

(24) Zhu, S.; Chen, Y.; Gao, X.; Lv, Z.; He, Y.; Wang, J.; Fan, W. Kraft lignin derived S and O co-doped porous graphene for metal-free benzylic alcohol oxidation. *Catal. Sci. Technol.* **2020**, *10*, 2786–2796.

(25) (a) Zhu, Y.; Li, Z.; Chen, J. Applications of lignin-derived catalysts for green synthesis. *Green Energy Environ.* **2019**, *4*, 210–244. (b) Suhas; Carrott, P. J. M.; Carrott, M. M. L. R. Lignin – from natural adsorbent to activated carbon: A review. *Bioresour. Technol.* **2007**, *98*, 2301–2312.

(26) Hayashi, J.; Kazehaya, A.; Muroyama, K.; Watkinson, A. P. Preparation of activated carbon from lignin by chemical activation. *Carbon* **2000**, *38*, 1873–1878.

(27) (a) Cardoso, B.; Mestre, A. S.; Carvalho, A. P.; Pires, J. Activated carbon derived from cork powder waste by KOH activation: Preparation, characterization, and VOCs adsorption. *Ind. Eng. Chem. Res.* **2008**, *47*, 5841–5846. (b) Molina-Sabio, M.; Rodríguez-Reinoso, F. Role of chemical activation in the development of carbon porosity. *Colloids Surf., A* **2004**, *241*, 15–25.

(28) Fierro, V.; Torné-Fernández, V.; Celzard, A. Methodical study of the chemical activation of Kraft lignin with KOH and NaOH. *Microporous Mesoporous Mater.* **2007**, *101*, 419–431.

(29) (a) Chen, W.; Gong, M.; Li, K.; Xia, M.; Chen, Z.; Xiao, H.; Fang, Y.; Chen, Y.; Yang, H.; Chen, H. Insight into KOH activation mechanism during biomass pyrolysis: Chemical reactions between O-containing groups and KOH. *Appl. Energy* **2020**, *278*, No. 115730. (b) Illingworth, J. M.; Rand, B.; Williams, P. T. Understanding the mechanism of two-step, pyrolysis-alkali chemical activation of fibrous biomass for the production of activated carbon fibre matting. *Fuel Process. Technol.* **2022**, *235*, No. 107348.

(30) Deng, J.; Xiong, T.; Xu, F.; Li, M.; Han, C.; Gong, Y.; Wang, H.; Wang, Y. Inspired by bread leavening: one-pot synthesis of

hierarchically porous carbon for supercapacitors. *Green Chem.* **2015**, *17*, 4053–4060.

(31) (a) Gerber, I.; Oubenali, M.; Bacsa, R.; Durand, J.; Gonçalves, A.; Pereira, M. F. R.; Jolibois, F.; Perrin, L.; Poteau, R.; Serp, P. Theoretical and experimental studies on the carbon-nanotube surface oxidation by nitric acid: Interplay between functionalization and vacancy enlargement. *Chem. − Eur. J.* **2011**, *17*, 11467–11477. (b) Li, J.; Ma, L.; Li, X.; Lu, C.; Liu, H. Effect of nitric acid pretreatment on the properties of activated carbon and supported palladium catalysts. *Ind. Eng. Chem. Res.* **2005**, *44*, 5478–5482.

(32) Ishimaru, K.; Hata, T.; Bronsveld, P.; Meier, D.; Imamura, Y. Spectroscopic analysis of carbonization behavior of wood, cellulose and lignin. *J. Mater. Sci.* **2007**, *42*, 122–129.

(33) González, D.; Altin, O.; Eser, S.; Garcia, A. B. Temperature-programmed oxidation studies of carbon materials prepared from anthracites by high temperature treatment. *Mater. Chem. Phys.* **2007**, *101*, 137–141.

(34) (a) Wirtanen, T.; Aikonen, S.; Muuronen, M.; Melchionna, M.; Kemell, M.; Davodi, F.; Kallio, T.; Hu, T.; Helaja, J. Carbocatalytic oxidative dehydrogenative couplings of (hetero)aryls by oxidized multi-walled carbon nanotubes in liquid phase. *Chem. − Eur. J.* **2019**, *25*, 12288–12293. (b) Casadio, D. S.; Aikonen, S.; Lenarda, A.; Nieger, M.; Hu, T.; Taubert, S.; Sundholm, D.; Muuronen, M.; Wirtanen, T.; Helaja, J. Divergent carbocatalytic routes in oxidative coupling of benzofused heteroaryl dimers: A mechanistic update. *Chem. − Eur. J.* **2021**, *27*, 5283–5291.

(35) Langley, L. A.; Villanueva, D. E.; Fairbrother, D. H. Quantification of surface oxides on carbonaceous materials. *Chem. Mater.* **2006**, *18*, 169–178.

(36) Powell, C. J.; Jablonski, A. Surface sensitivity of X-ray photoelectron spectroscopy. *Nucl. Instrum. Methods Phys. Res., Sect. A* **2009**, *601*, 54–65.

(37) Cuesta, A.; Dhamelincourt, P.; Laureyns, J.; Martinez-Alonso, A.; Tascón, J. M. D. Raman microprobe studies on carbon materials. *Carbon* **1994**, *32*, 1523–1532.

(38) Presolski, S.; Pumera, M. Graphene oxide: Carbocatalyst or reagent? *Angew. Chem., Int. Ed.* **2018**, *57*, 16713–16715.

(39) (a) Espinosa, J. C.; Álvaro, M.; Dhakshinamoorthy, A.; Navalón, S.; García, H. Engineering active sites in reduced graphene oxide: Tuning the catalytic activity for aerobic oxidation. *ACS Sustainable Chem. Eng.* **2019**, *7*, 15948–15956. (b) Li, X.-H.; Chen, J.-S.; Wang, X.; Sun, J.; Antonietti, M. Metal-free activation of dioxygen by graphene/g-C$_3$N$_4$ nanocomposites: Functional dyads for selective oxidation of saturated hydrocarbons. *J. Am. Chem. Soc.* **2011**, *133*, 8074–8077.

(40) Mollar-Cuni, A.; Ventura-Espinosa, D.; Martín, S.; García, H.; Mata, J. A. Reduced graphene oxides as carbocatalysts in acceptorless dehydrogenation of N-heterocycles. *ACS Catal.* **2021**, *11*, 14688–14693.

(41) Wu, H.; Su, C.; Tandiana, R.; Liu, C.; Qiu, C.; Bao, Y.; Wu, J.; Xu, Y.; Lu, J.; Fan, D.; Loh, K. P. Graphene-oxide-catalyzed direct CH−CH-type cross-coupling: The intrinsic catalytic activities of zigzag edges. *Angew. Chem., Int. Ed.* **2018**, *57*, 10848–10853.

(42) Lv, G.; Wang, H.; Yang, Y.; Deng, T.; Chen, C.; Zhu, Y.; Hou, X. Graphene oxide: A convenient metal-free carbocatalyst for facilitating aerobic oxidation of 5-hydroxymethylfurfural into 2,5-diformylfuran. *ACS Catal.* **2015**, *5*, 5636–5646.

(43) Shibuya, M.; Tomizawa, M.; Suzuki, I.; Iwabuchi, Y. 2-Azaadamantane N-oxyl (AZADO) and 1-Me-AZADO: Highly efficient organocatalysts for oxidation of alcohols. *J. Am. Chem. Soc.* **2006**, *128*, 8412–8413.

(44) Tang, P.; Hu, G.; Li, M.; Ma, D. Graphene-based metal-free catalysts for catalytic reactions in the liquid phase. *ACS Catal.* **2016**, *6*, 6948–6958.

(45) Trogen, M.; Le, N.-D.; Sawada, D.; Guizani, C.; Lourençon, T. V.; Pitkänen, L.; Sixta, H.; Shah, R.; O'Neill, H.; Balakshin, M.; Byrne, N.; Hummel, M. Cellulose-lignin composite fibres as precursors for carbon fibres. Part 1 − Manufacturing and properties of precursor fibres. *Carbohydr. Polym.* **2021**, *252*, No. 117133.